Numerical study of the influence of internal structural design on the thermal performance of hollow brick configurations based on HCB8-brick

Ibtissam Lamaamar [1*], *Khadija* Choukairy [1], *Oumayma* Babaharra [2,3], *Kaoutar* Khallaki [1], *Hafid* El Kharaz [4]

[1] Sultan Moulay Slimane University, Laboratory of Process, Energy, Materials and Environment, ENSA Khouribga, Morocco
[2]Higher School of Technology, Ibn Zohr University, Laâyoune, Morocco
[3]Laboratory of Mechanics, Processes, Energy and Environment, National School of Applied Sciences, Ibn Zohr University, Morocco
[4]Hassan II University, Laboratory of Modelling and Simulation of Intelligent Industrial Systems, ENSET Mohammedia, Morocco

Abstract. This study aims to compare and evaluate five hollow brick configurations with different internal structures, derived from a reference brick (HCB8), in order to identify the configuration providing the best thermal insulation performance under the studied conditions. The results show that the internal distribution of the solid material and air significantly affects the thermal resistance and that the performance ranking of the configurations varies depending on the operating parameters. The configurations conf-5 and conf-4 offer the best thermal insulation for k =0.207 W/ m .K and k=0.925 W/ m .K respectively. Replacing air by EPS or PUF, conf-4 offers the best thermal performance, followed by conf-2, generally the least efficient in terms of insulation. These results highlight the importance of taking outdoor conditions and material properties into account in thermal analysis, as they can significantly alter the ranking of geometric performance.

Keywords: Hollow brick, Heat transfer; Internal geometry, Thermal insulation

* Corresponding author: ibtissamlamaamar@gmail.com

Nomenclature		**Subscript**	
ρ	Density (Kg/ m^3)	B	Bottom
C_p	Specific heat (J/Kg.K)	T	Top
k	Thermal conductivity (W/ m .K)	h	Horizontal
T	Temperature (K)	p	Perpendicular
R_{Th}	Thermal resistance (K-m²/W)	e	Spacing
α	Diffusivity (m^2/s)	St	Stream temperature
h	Heat transfer coefficient (W/m^2 K)	w	wall
μ	Dynamic Viscosity (Kg/m.s)	adj	Adjusted
g	Acceleration of gravity (m/s^2)	ref	Reference
β	Thermal expansion coefficient (1/K)	out	outside
$\overline{V}$	Average velocity (m/s)	int	Internal
ψ	Stream function	confs	Configurations
		EPS	Expanded polystyrene
		PUF	Polyurethane foam

1 Introduction

Managing heat transfer within the building envelope is a major global challenge, both in terms of thermal comfort and reducing energy consumption in buildings. This sector accounts for more than 36%of global energy consumption and nearly 37% of emissions of CO_2 associated with it [1] In regions characterized by significant climatic contrasts, homes are particularly exposed to seasonal variations, leading to significant thermal discomfort when walls are not adapted [2], [3]

Among the various components of the building envelope, improving the insulation of walls remains one of the most effective ways to reduce energy requirements for heating and air conditioning. Several strategies exist, i) interior insulation, which is protected from the elements but may pose a risk in the event of a fire; ii) exterior insulation, which generally offers the best thermal continuity but involves high costs and technical constraints; iii) cavity insulation, which is limited by the available space and potentially affected by moisture or material settling [2]–[4]

In many countries, masonry systems such as hollow clay bricks or concrete masonry units (CMUs) are particularly widespread due to their low cost, local availability, and ease of use. In Morocco, for example, hollow bricks with 8 or 12 cavities are gradually replacing traditional solid blocks due to their light weight, moderate cost, and ability to improve the thermal performance of buildings [5]. However, the actual insulating efficiency of these elements is strongly influenced by the geometry of the internal cells. These cells not only induce conduction through the solid walls, but also convective movements in the trapped air, as well as radiative exchanges between internal walls. These mechanisms sometimes significantly degrade the nominal thermal resistance of the brick or block [6]

The integration of insulation, modification of internal shapes such as rhomboidal cavities, multi-chamber cells, and addition of protuberances have been shown to reduce energy exchange through complementary mechanisms, reduction of conductive paths, inhibition or reorientation of convective movements, and reduction of radiative exchange through low-emissivity surfaces, sometimes without a noticeable increase in weight or manufacturing cost [7]–[10].

However, improvements to internal geometry must comply with regulatory and mechanical constraints. For example, structural bricks must meet strict requirements regarding the percentage of solid area, minimum wall thickness, dimensions, and distribution of internal cavities. These constraints severely limit the freedom to design geometries that simultaneously optimize thermal performance and mechanical strength. This results in a delicate compromise between insulation, structural stability, and industrial feasibility [10]
Recent studies aimed at characterizing the thermal behavior of cellular masonry have shown the value of combining experimental measurements (particularly using hot-box devices) with advanced three-dimensional modeling based on CFD coupled with heat transfer. This dual approach has made it possible, in the literature, to compare numerical predictions with experimental data and thus establish reliable models capable of reproducing the mechanisms of conduction, internal convection, and radiation present in the cavities. Based on this validated work, numerical analysis is now a robust tool for exploring a wide range of scenarios that are not accessible experimentally. In particular, it allows for parametric evaluation of the influence of the internal geometry of the cells, the thermophysical properties of the materials, the possible introduction of insulating materials into the cavities, and the radiative characteristics of the internal surfaces [11], [12].
In this context, the present study is based exclusively on a two-dimensional numerical analysis aimed at characterizing the thermal behavior of different internal structures of hollow bricks. Using detailed CFD models that simultaneously integrate conduction, convection, and radiation, it parametrically examines the influence of thermal conductivity of the constituent material, , and the type of material that may be introduced into the cavities. Two filling materials, expanded polystyrene (EPS) and polyurethane foam (PUF), were also compared with air in order to assess their influence on the thermal performance of the different structures This approach makes it possible to identify the configurations offering the best energy performance while taking into account real geometric and construction constraints.

2 Methods and Materials

2.1 Physical model

The physical model studied represents a hollow brick with external dimensions of 19 cm × 10 cm [5], subjected to convective heat flow at both ends. Each geometric configuration is defined by a different distribution of air and solid material, allowing the effect of the internal structure on overall thermal behavior to be evaluated. Figure 1 shows the different configurations studied and Table 1 presents the different sizes of configurations. The thermal conductivity, specific heat, and density of the materials are selected from values commonly accepted in the literature (see Table 2). A thermal analysis was carried out to study the thermal behavior of each configuration and evaluate the evolution of their performance as a function of the thermal conductivity of solid material, and filling materials which are EPS and PUF.

Table 1. Sizing of the proposed configurations

No. configurations	$e_{int,ext}$ **(cm)**	$e_{ins,h}$ **(cm)**	**Cavity length (cm)**	**Cavity Large (cm)**	**Protuberance thickness (cm)**	**Protuberance length (cm)**	**Cavity number**
Conf-Ref	1	1	3.5	3.5	-	-	8

Conf-1	1	1	8	3.5	-	-	4
Conf-2	1	1	17	3.5	-	-	2
Conf-3	0.75	0.75	3.5	2.33			12
Conf-4	0.75	0.75	17	2.33	-	-	3
Conf-5	0.75	0.75	3.5	2.33	0.5	3	12

Table 2. Thermophysical proprieties, of materials [5], [13]

Materials	**Density (Kg/ m^3)**	**Specific heat (J/Kg.K)**	**Thermal conductivity (W/ m .K)**	**Dynamic Viscosity (Kg/(m.s))**	**Thermal expansion coefficient (1/K)**
Air	1.225	1001.43	0.026	$0.846.10^{-5}$	0.0035
Clay	664	741	0.207	-	-
EPS	22	1280	0.041	-	-
PUF	417	1400	0.0605	-	-

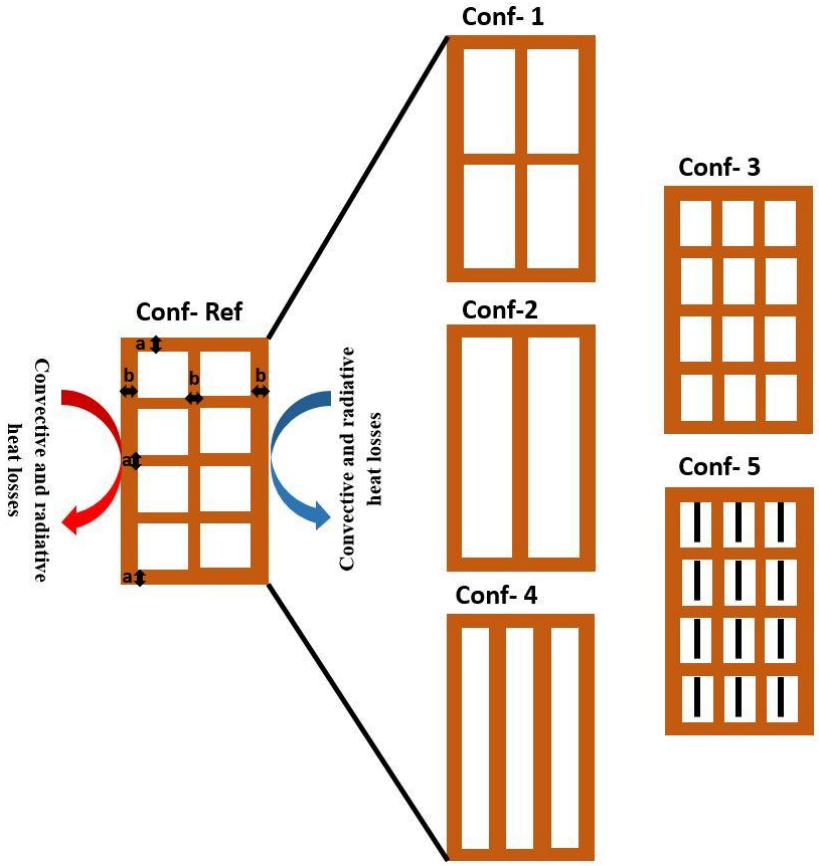

Figure 1. Physical model of different configurations

2.2 Assumptions

The model is developed under the following assumptions: (i) the air flow within the cavities is laminar, incompressible, and characterized by low velocities; (ii) the thermophysical properties of each material are assumed to be constant; (iii) internal heat generation is neglected; and (iv) the analysis is conducted under a two-dimensional framework.

2.3 Mathematical modelling and boundary conditions

The overall thermal behavior of the system is based on the equations of conservation of mass, momentum, and energy, applied to the solid medium and the air contained in the cavities. Conductive, convective, and radiative exchanges are taken into account. Under these assumptions, the energy equation for solids, the Navier–Stokes equation for air, the mass conservation equation, the surface-to-surface radiation flux, and boundary conditions are summarized below.

Solid part

$$k\left(\frac{\partial^2 T}{\partial^2 x}+\frac{\partial^2 T}{\partial^2 y}\right)=0 \quad (1)$$

Navier–Stokes equation for air, the mass conservation equation,

$$\frac{\partial u}{\partial x}+\frac{\partial v}{\partial y}=0 \quad (2)$$

$$u\frac{\partial u}{\partial x}+v\frac{\partial u}{\partial y}=\frac{1}{\rho_{air}}\left[-\frac{\partial p}{\partial x}+\mu_{air}*\left(\frac{\partial^2 u}{\partial x^2}+\frac{\partial^2 u}{\partial y^2}\right)\right] \quad (3)$$

$$u\frac{\partial v}{\partial x}+v\frac{\partial v}{\partial y}=\frac{1}{\rho_{air}}\left[-\frac{\partial p}{\partial y}+\mu_{air}*\left(\frac{\partial^2 v}{\partial x^2}+\frac{\partial^2 v}{\partial y^2}\right)+(\rho\beta)_{air}g\Delta T\right. \quad (4)$$

$$u\frac{\partial T}{\partial x}+v\frac{\partial T}{\partial y}=\frac{\lambda_{air}}{\rho_{air}C_{p,air}}\left[\left(\frac{\partial^2 T}{\partial x^2}+\frac{\partial^2 T}{\partial y^2}\right)\right] \quad (5)$$

Radiation equation

$$q_{r,i}(r_i)=B_j(r_j)-\sum_{\substack{i=1\\ j\neq i}}^{4}\int_{S_j}B_j(r_j)k(r_i,r_j)dS_j, i=1\ldots4 \quad (6)$$

Boundary conditions

At outside, with $h_{out}=20$ W/ m^2 K [14]

$$-k_{brick}\frac{\partial T}{\partial x}=h_{out}(T_{st,out}-T_{w,out}) \quad (7)$$

At inside ,with $h_{int}=5$ W/ m^2 K [14]

$$-k_{brick}\frac{\partial T}{\partial x}=h_{int}(T_{st,int}-T_{w,int}) \quad (8)$$

2.4 Model validation and numerical solution method

The numerical model was previously verified by comparing it with numerical results of Laaroussi et al.[15], on hollow brick subjected to a similar heat flux. The temperature distributions in Figure 2 and heat flux values obtained are in good agreement with the references with relative errors of 0.6%. The numerical resolution is performed in steady state using a solver based on the finite volume method. After a mesh independence study, a grid

of 119,621 cells was selected, offering a good compromise between geometric fineness and computational cost (see Table 3). The momentum and energy equations are solved using a coupled scheme, adapted to the Boussinesq approximation used to represent buoyancy effects in air cavities. The convergence criterion is set at 10^8 for velocity, pressure, and temperature, ensuring a stable and numerically accurate solution. Spatial discretization is performed using a second-order implicit scheme, allowing for better representation of thermal and dynamic gradients. All calculations were performed in double precision on a machine equipped with an Intel® Xeon® processor, 16 GB of RAM at 3.5 GHz, in single-process mode.

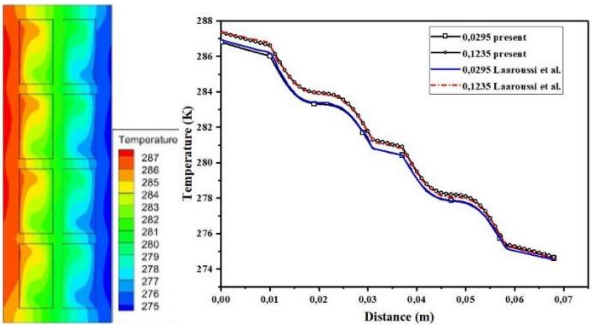

Figure 2. Isotherms and temperature distribution for different lines horizontal for vertical position

. Table 3. Mesh independence analysis based on heat flow

Elements	30287	76000	119621	211189
∅ (W/m^2)	30.27	30.2557	30.2509	30.2496
Abs diff (%) of ∅	0.0097	0.057	0.073	0.077

3 Results and discussions

3.1 Effect of geometry

We studied the thermal behavior of six bricks with different internal geometries, all measuring 190 mm × 100 mm, made from the same materials (clay) and subjected to the same boundary conditions. The outside air temperature is set at 317 K, the inside air temperature at 298 K, with heat transfer coefficients of 20 W/m²K on the outside and 5 W/m²K on the inside [14]. Inside the cavities, the three modes of transfer conduction, convection, and radiation are taken into account, considering an internal emissivity of 0.9 [15]. The effect of geometry was evaluated by comparing each configuration to the reference brick (conf-ref). The results show that thermal resistance is highly sensitive to internal geometry. It reaches a maximum of 0.749 K·m²/W for the conf-5 configuration and a minimum of 0.432 K·m²/W for conf-3, revealing the decisive influence of the shape and arrangement of the cavities on thermal performance. Although all bricks are subjected to the same operating conditions, their behavior differs greatly due to variations in air percentage, solid material distribution, and internal morphology. Analysis of isotherms and heat flows provides insight into the mechanisms governing these differences.

Depending on the configuration, the simple distribution of the material can either improve or degrade heat transfer by altering the balance between conductive, convective, and radiative flows (Table 4). For example, conf-1 characterized by high–aspect ratio cavities that promote

strong internal air movement, show a decrease in performance (-6%). These geometries promote air circulation, increasing convective transfer along the walls and intensifying radiative exchange, leading to a more curved heat transfer (see Figure 3 and Figure 4), which degrades thermal resistance. This effect is further reinforced in the conf-2 configuration, where only the heights of the cavities increase.

For configurations conf-3 and conf-4 with three columns, increasing the aspect ratio (from 3.5/2.333 to 17/2.333) results in a slight decrease in performance (+19% to +17%), which is due to improved in radiative transfer in conf-4. In general, analysis of configurations conf-1 to conf-4 shows that the beneficial effect of aspect ratio on thermal performance is achieved when the width of the cavities remains proportional to their length. A balanced control between these two dimensions is therefore essential to take full advantage of the elongation of the cavities.

Finally, adding protuberances to the conf-5 geometry leads to a significant improvement in thermal resistance. These elements further attenuate internal convection, with the air being almost stagnant, with a maximum stream function of 0.00005 (Figure 4), which traps the air, revealing a near-zero flow, and greatly reduces convective and radiative exchanges.. Heat transfer in the brick becomes very similar to pure conduction transfer (see Figure 3), which explains the significant increase in performance.

In conclusion, these results demonstrate that the internal geometry of bricks is a major lever for thermal optimization: by controlling the shape and distribution of cavities, it is possible to effectively reduce convective and radiative transfers, thereby improving the overall thermal resistance of the building element.

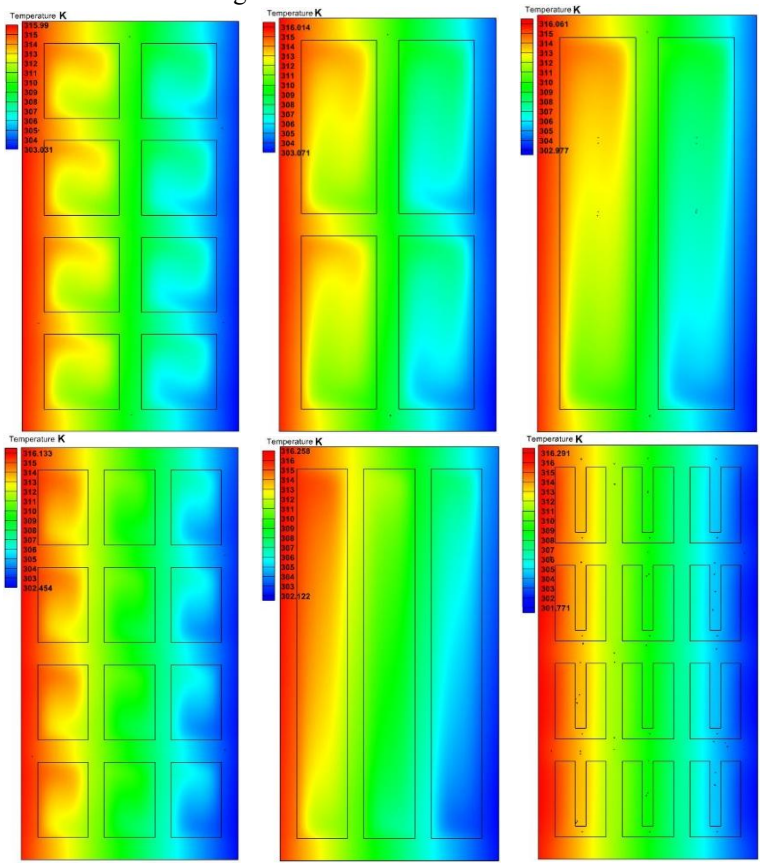

Figure 3. Contours of temperature

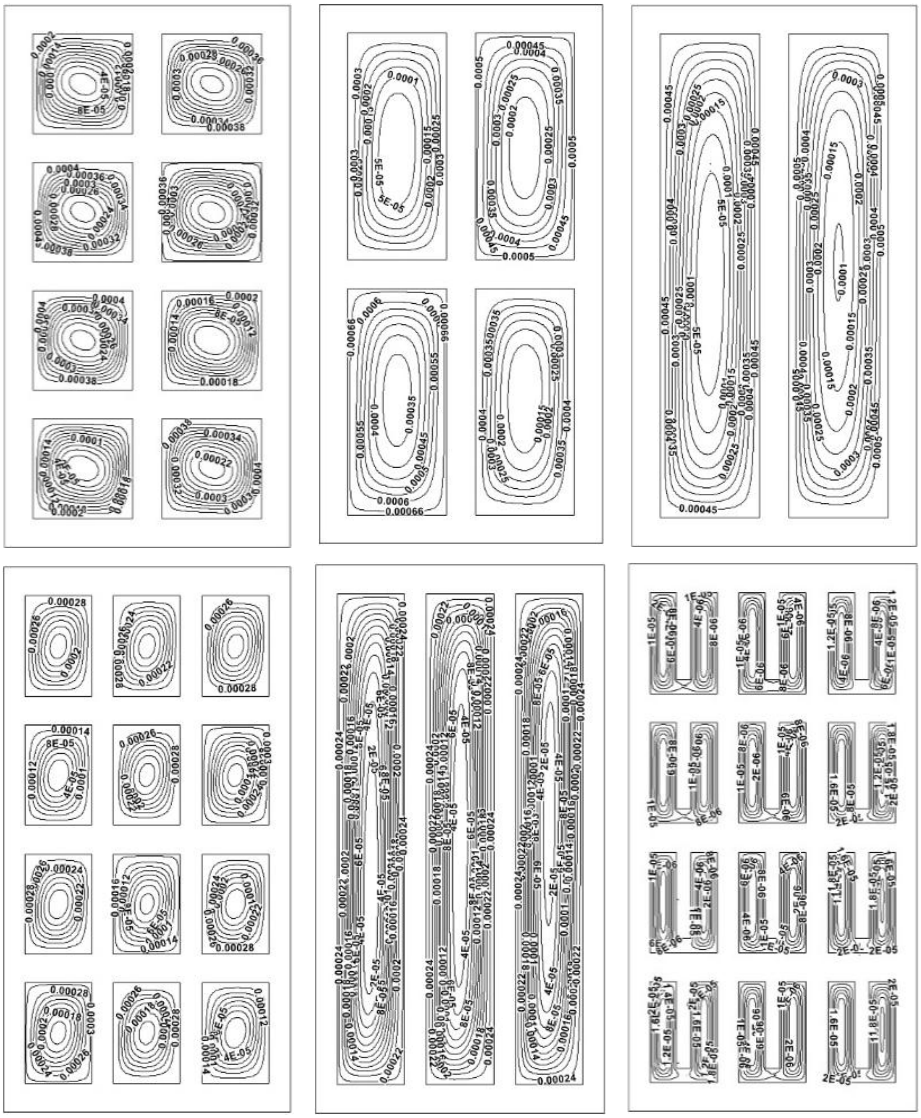

Figure 4. Stream function of configurations

Table 4. Heat flux percentage and thermal resistance and geometric proprieties

Configurations	$Flux_{conv+cond}$	$Flux_{rad}$	R_{th}	Diff in R_{th} %	Solid percentage %	Air percentage %
Conf-Ref	68%	32%	0.474	0%	48.42	51.58
Conf-1	62%	38%	0.443	-6%	41.05	58.95
Conf-2	58,93%	41,07%	0.432	-8.80%	37.37%	62,63

Conf-3	67%	33%	0.565	19%	48.49	51.5
Conf-4	55%	45%	0.558	17%	37.378	62.622
Conf-5	72%	28%	0.749	58%	57.97	42.031

3.2 Effect of thermal conductivity

Analysis of the two thermal conductivities tested highlights a very different thermal behavior of the configurations depending on whether conduction in the solid material is low (k = 0.207 W/m·K) or, on the contrary, dominant (k = 0.925 W/m·K). When conductivity is high, heat flows more easily through the walls, which makes the thermal resistance lower for higher conductivities as is shown in Figure 5. According to Table 5, the relative difference in thermal resistance reaches a maximum of 58% for configuration 5 with k = 0.207 W/m·K, and 60% for configuration 4 with k = 0.925 W/m·K. This result shows that configurations with cavities exhibiting a high aspect ratio become significantly more efficient when the thermal conductivity of the solid is high. Indeed, these geometries impose a longer and more complex path for heat within the material, which limits the heat flux even if the material is a strong conductor of heat. This is why configurations Conf-1, Conf-2, and Conf-4, show significant improvements when k = 0.925.
Furthermore, for high conductivity, small geometric variations do not have a noticeable effect on thermal resistance, in contrast to low conductivities, where even a small change leads to an improvement. For example, the transition from Conf-3 to Conf-5 increases the relative improvement from 17% to 58% for k = 0.207, and from 15% to 33% for k = 0.925. This confirms that, for low conductivity, a good solid/air distribution and well-positioned protuberances effectively increase thermal resistance, as they simultaneously limit convective and radiative losses, thus significantly increasing thermal resistance. Conversely, for high conductivity, only geometries offering a significantly elongated solid path produce a marked improvement. In addition, the thermal conductivity of the material has a decisive influence on the ability of each geometry to mobilize its internal conduction paths. A change in the material can thus reverse the order of efficiency between configurations, as described in Table 6.

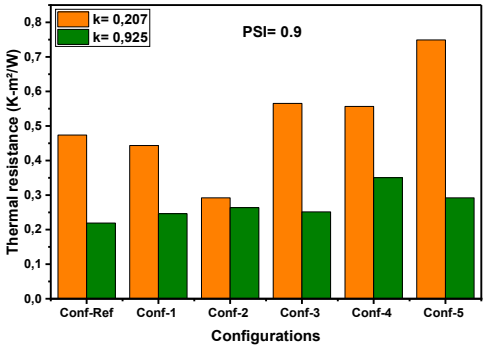

Figure 5. Thermal resistance as function of configurations for different thermal conductivities

Table 5. Relative difference in thermal resistance of different configurations

Thermal conductivity (W/m K)	Conf-Ref	Conf-1	Conf-2	Conf-3	Conf-4	Conf-5
K= 0,207	-	-6%	-9%	19%	17%	58%
K= 0,925	-	12%	20%	15%	60%	33%

Table 6. Order of configuration performance based on thermal resistance for different thermal conductivities

Thermal conductivity (W/m K)	Performance order of Configurations					
k=0,207	Conf-5	Conf-3	Conf-4	Conf-Ref	Conf-1	Conf-2
k=0,925	Conf-4	Conf-5	Conf-2	Conf-3	Conf-1	Conf-Ref

3.3 Effect of filling material

Figure 7 shows the thermal resistance of the different configurations studied with three filling materials: EPS, PUF, and air. It is clear that EPS stands out for its significantly superior performance, as it achieves the highest thermal resistance. This efficiency can be explained by its very low thermal conductivity, which is particularly effective at limiting heat transfer by conduction. PUF comes in second place, with satisfactory results but slightly less good than those of EPS. As for air, it appears to be the least efficient material, its insulating capacity is lower due to the mobility of air in the cavities, which promotes internal convective movements. According to Figure 7, the evolution of thermal resistance as a function of the percentage of solid material shows that, for insulating materials such as EPS and PUF, the general trend is for a gradual decrease in thermal resistance as the solid fraction increases. It can also be seen that configurations with the same solid material content generally have similar thermal performance. On the other hand, when air is used as a filler, the dispersion of results is much greater. Configurations with the same solid fraction exhibit very different thermal resistances. This behavior highlights the major impact of the internal geometry of cavities on convective transfers in the case of air, unlike solid insulators where conduction predominates and tends to make the results more uniform.

Analysis of Table 7 also confirms that the ranking of configurations is not universal: it depends heavily on the filling material. A highly efficient configuration with EPS or PUF can give much lower results when filled with air or another material. This highlights the complex nature of the interaction between the internal geometry and the specific properties of the filling material, an interaction that becomes a determining factor in overall thermal behavior.

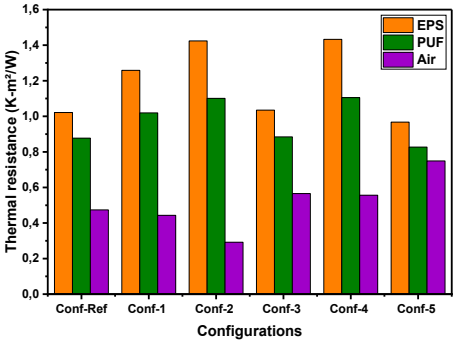

Figure 6. Variation of thermal resistance a) as function of configurations with different filling materials

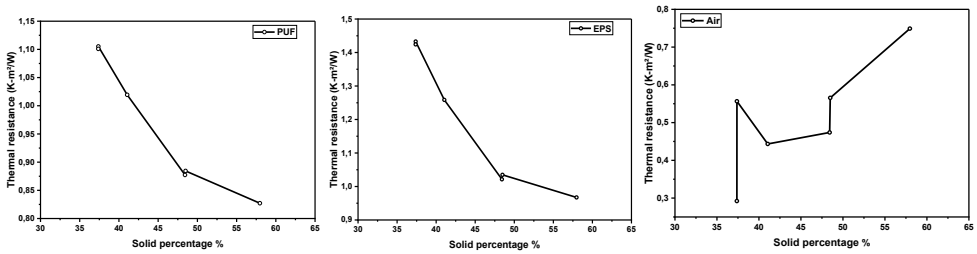

Figure 7. Internal temperature variation with solid percentage

Table 7. Order of configuration performance based on thermal resistance for different filling materials

Filling materials	Performance order of Configurations					
EPS	Conf-4	Conf-2	Conf-1	Conf-3	Conf-Ref	Conf-5
PUF	Conf-4	Conf-2	Conf-1	Conf-3	Conf-Ref	Conf-5
Air	Conf-5	Conf-3	Conf-4	Conf-Ref	Conf-1	Conf-2

4 Conclusion

This two-dimensional numerical study demonstrated that the internal geometry of bricks has a decisive influence on their thermal behavior. Five internal structures, derived from the reference hollow brick with eight cavities, showed that the shape of the cavities, their distribution, and the integration of protrusions significantly modify transfers by conduction, convection, and radiation. Configurations with elongated cavities or internal barriers offer the best performance, while wide, sparsely divided cavities promote convective and radiative exchange, thereby reducing thermal resistance. The analysis also reveals that the ranking of configurations can change depending on operating conditions like the filling material and the conductivity of brick. These results provide a solid basis for the design of energy-efficient bricks adapted to different climatic and construction contexts.

References

[1] M. Santamouris and K. Vasilakopoulou, Present and future energy consumption of buildings : Challenges and opportunities towards decarbonisation. e-Prime - Adv. Electr. Eng. Electron. Energy. vol. 1, 100002, (2021). https://doi.org/10.1016/j.prime.2021.100002

[2] P. M. Cuce, E. Cuce, and K. Sudhakar, A systematic review of thermal insulation performance of hollow bricks as a function of hollow geometry. Int. J. Ambient Energy. vol. 43, 4406–4415, (2022). https://doi.org/10.1080/01430750.2021.1907619

[3] A. Bouchair, Steady state theoretical model of fired clay hollow bricks for enhanced external wall thermal insulation. Build. Environ. vol. 43, 1603–1618, (2008). https://doi.org/10.1016/j.buildenv.2007.10.005

[4] E. Cuce, P. M. Cuce, and A. B. Besir, Improving thermal resistance of lightweight concrete hollow bricks: A numerical optimisation research for a typical masonry unit. J. Energy Syst. vol. 4, 121–144, (2020). https://doi.org/10.30521/jes.775961

[5] S. Hamdaoui, A. Bouchikhi, M. Azouggagh, M. Akour, A. Ait Msaad, and M.

Mahdaoui, Building hollow clay bricks embedding phase change material: Thermal behavior analysis under hot climate. Sol. Energy, vol. 237, 122–134, (2022). https://doi.org/10.1016/j.solener.2022.03.073

[6] B. Jamal, M. Boukendil, L. El, A. Abdelbaki, and Z. Zrikem, Numerical investigation of combined heat transfer through hollow brick walls. Eur. Phys. J. Plus. vol. 123, (2020). https://doi.org/10.1140/epjp/s13360-020-00840-8

[7] V. A. F. Costa, Improving the thermal performance of red clay holed bricks. Energy Build. vol. 70, 352–364, (2014). https://doi.org/10.1016/j.enbuild.2013.11.052

[8] K. Arendt, M. Krzaczek, and J. Florczuk, Numerical analysis by FEM and analytical study of the dynamic thermal behavior of hollow bricks with different cavity concentration. Int. J. Therm. Sci. vol. 50, 1543–1553, (2011). https://doi.org/10.1016/j.ijthermalsci.2011.02.027

[9] L. P. Li, Z. G. Wu, Z. Y. Li, Y. L. He, and W. Q. Tao, Numerical thermal optimization of the configuration of multi-holed clay bricks used for constructing building walls by the finite volume method. Int. J. Heat Mass Transf. vol. 51, 3669–3682, (2008). https://doi.org/10.1016/j.ijheatmasstransfer.2007.06.008

[10] S. Vera, C. Figueroa, S. Chubretovic, J. C. Remesar, and F. Vargas, Improvement of the thermal performance of hollow clay bricks for structural masonry walls. Constr. Build. Mater. vol. 415, 135060, (2024). https://doi.org/10.1016/j.conbuildmat.2024.135060

[11] M. Martínez, N. Huygen, J. Sanders, and S. Atamturktur, Thermo-fluid dynamic analysis of concrete masonry units via experimental testing and numerical modeling. J. Build. Eng. vol. 19, 80–90, (2018). https://doi.org/10.1016/j.jobe.2018.04.029

[12] A. S. Al-Tamimi, O. S. Baghabra Al-Amoudi, M. A. Al-Osta, M. R. Ali, and A. Ahmad, Effect of insulation materials and cavity layout on heat transfer of concrete masonry hollow blocks. Constr. Build. Mater. vol. 254, 119300, (2020). https://doi.org/10.1016/j.conbuildmat.2020.119300

[13] O. Babaharra, K. Choukairy, K. Khallaki, and S. Hayani Mounir, Numerical study of phase change material microencapsulated in a typical multilayer wall for a hot climatic zone. Heat Transf. vol. 51, 1193–1212, (2022). https://doi.org/10.1002/htj.22348

[14] O. Babaharra, K. Choukairy, H. Faraji, K. Khallaki, S. Hamdaoui, and Y. Bahammou, Thermal performance analysis of hollow bricks integrated phase change materials for various climate zones. Heat Transf. vol. 53, 2148–2172, (2024). https://doi.org/10.1002/htj.23031

[15] N. Laaroussi, G. Lauriat, S. Raefat, M. Garoum, and M. Ahachad, An example of comparison between ISO Norm calculations and full CFD simulations of thermal performances of hollow bricks. J. Build. Eng. vol. 11, 69–81, (2017). https://doi.org/10.1016/j.jobe.2017.03.011